ACS MATERIALS LETTERS

www.acsmaterialsletters.org

# Direct Synthesis of Highly Siliceous ZnO-FAU Zeolite with Enhanced Performance in Hydrocarbon Cracking Reactions

Deependra Parmar, Adam J. Mallette, Noemi Linares, Sarah A. Saslow, Tanguy Terlier, James J. Strohm, Lee P. Barber, Heng Dai, Javier García-Martínez, and Jeffrey D. Rimer*

Cite This: ACS Materials Lett. 2023, 5, 202−208

Read Online

ACCESS | Metrics & More | Article Recommendations | Supporting Information

**ABSTRACT:** **The hydrothermal stability and catalytic activity of zeolite Y (faujasite, FAU) is highly dependent on its composition. High silicon content is often desirable for catalytic applications; however, direct synthesis of faujasite with high silicon content (Si/Al > 2.5) is nontrivial. Here, we present an organic-free synthesis of FAU-type zeolite with Si/Al = 3.4 using zinc oxide as a modifier. A combination of spectroscopy and microscopy techniques confirms that ZnO is well-distributed within zeolite pores as extra-framework species, and the nature of these species differs from bulk ZnO and framework zinc in Zn-FAU crystals. We demonstrate that the increased Si/Al ratio leads to improved hydrothermal stability, while catalytic cracking of 1-hexene and cumene show that ZnO-FAU exhibits a significantly longer lifetime compared to in-house and commercial zeolite Y. Collectively, this study presents a facile and efficient method to prepare more siliceous FAU with enhanced catalytic performance.**

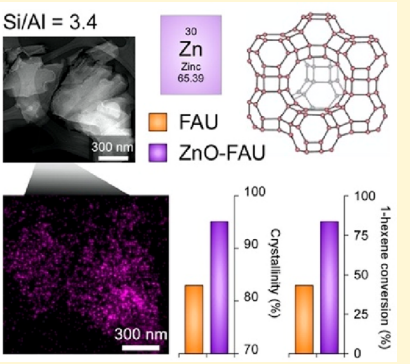


Zeolites are microporous (alumino)silicate materials that are ideal heterogeneous catalysts owing to their shape selectivity and exceptional physicochemical properties.[1] One of the most commercially relevant zeolite catalysts is faujasite (FAU).[2] These materials are commonly classified on the basis of their Si/Al ratio, which include low-silica zeolite X (LSX, Si/Al ≈ 1), zeolite X (1 < Si/Al < 1.5), zeolite Y (1.5 < Si/Al < 3), and ultrastable zeolite Y (USY, Si/Al > 3).[3] USY with Si/Al > 6 is the most widely used zeolite for fluidized catalytic cracking (FCC) in petroleum refining.[4] Direct synthesis of USY is challenging, and thus its preparation usually requires dealumination of zeolite Y (among other steps) to achieve a material that possesses the hydrothermal stability and activity necessary for cracking or other reactions.[5] Prior studies for the direct synthesis of FAU crystals with high silicon content have focused on bottom-up methods. To our knowledge, the highest reported value is Si/Al = 9;[6] however, the majority of direct FAU syntheses require organic structure-directing agents (OSDAs), such as 15-crown-5 ether[7] or tetraalkylammonium cations,[8,9] and/or unusual synthesis conditions that are nonideal for commercial processes, such as high temperature and the use of organosilanes.[9,10] We previously reported the synthesis of HOU-3 (FAU type) with the highest silicon content (Si/Al = 3) achieved without the use of an OSDA, crystal seeds, or a fluoride growth medium.[11] It has also been demonstrated that FAU syntheses with inorganic additives, such as ZnO,[12] $Co^{2+}$,[13] or •OH radicals,[9] can influence zeolite Y formation to yield higher Si/Al ratios with a concomitant enhancement of catalytic performance.[14]

In this study, we present a synthesis of zeolite Y with one of the highest silicon contents (Si/Al = 3.4) prepared by a one-pot, organic-free method in hydroxide growth media. Our approach utilizes zinc oxide as an inorganic additive to generate a ZnO-faujasite product where zinc is an extra-framework species well-distributed throughout the pores. We use a combination of steaming tests and multiple cracking reactions to demonstrate that the reduced aluminum content (and Brønsted acidity) of ZnO-faujasite results in improved hydrothermal stability and enhanced catalytic activity compared to both in-house and commercial zeolite Y.

Faujasite is conventionally synthesized in highly alkaline media (blue region in Figure 1A) to yield products with relatively low silicon content (Si/Al ≤ 2.5).[15] The synthesis of high-silica HOU-3 involved a reduced alkalinity, higher silica

Received: October 16, 2022
Accepted: December 7, 2022
Published: December 14, 2022

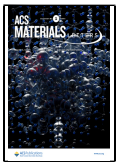






https://doi.org/10.1021/acsmaterialslett.2c00978
ACS Materials Lett. 2023, 5, 202−208

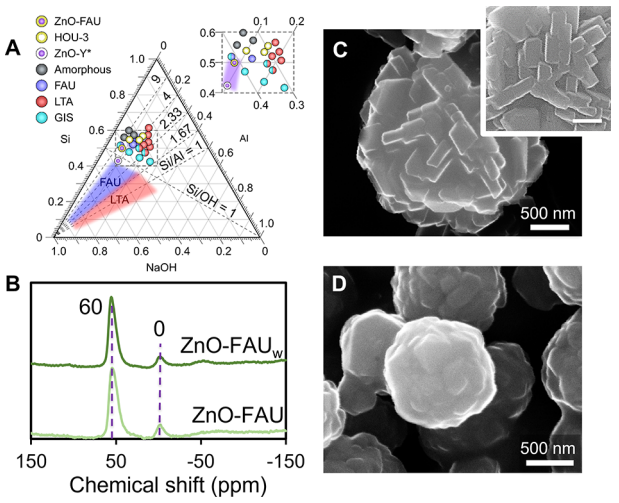


**Figure 1. (A) Ternary phase diagram adapted from Oleksiak et al.[15] showing products from organic-free syntheses. Symbols correspond to materials synthesized at 100 °C, with the exception of ZnO-Y* that was taken from Wang et al.[9] The blue and red shaded regions correspond to FAU and LTA synthesis at 65 °C, respectively. (B) Solid-state $^{27}$Al MAS NMR spectra of ZnO-faujasite samples prepared at 100 °C before (ZnO-FAU) and after (ZnO-FAU$_W$) mild acid washing showing peaks for tetrahedral Al (60 ppm) and octahedral Al (0 ppm). (C and D) Scanning electron micrographs of FAU crystals from (C) ZnO-assisted (ZnO-FAU) and (D) ZnO-free (FAU$_{syn}$) syntheses. Inset in C: Magnified image of a ZnO-FAU aggregate showing nanocrystals with sizes spanning from 200 to 400 nm (scale bar equals 400 nm).**

concentration, and a higher temperature (100 °C) than typical FAU syntheses.[11] In this study, we further extend the compositional space (i.e., Si/Al ratio) of this zeolite by adding zinc oxide (ZnO) to a modified HOU-3 synthesis gel (Figure 1A). The product of this synthesis is a ZnO-FAU material (Figures 1A and S1) with the lowest aluminum content (Si/Al = 3.4) reported in the absence of organics, crystal seeds, or fluoride. Powder X-ray diffraction (XRD) confirmed the crystallinity of ZnO-FAU (Figure S1) while the overall composition (Table 1) was validated using energy dispersive X-ray spectroscopy (EDS).

A parametric study of multiple synthesis parameters (Figure S2) revealed that the most effective method to control Si/Al ratio involves tuning the alkalinity and ZnO content. A higher hydroxide concentration promotes the formation of more crystalline FAU with lower Si/Al ratio. On the contrary, increasing the ZnO concentration leads to FAU products with lower crystallinity and higher Si/Al ratios. Attempts to increase the rate of nucleation by adding zeolite seeds were successful but resulted in products with lower Si/Al ratios (Figure S3), while increasing temperature resulted in the formation of zeolite GIS impurity above 100 °C (Table S1 and Figure S4). A FAU-to-GIS interzeolite transformation is commonly reported at 100 °C;[16] however, our results align with previous studies demonstrating that the presence of zinc in growth media stabilizes zeolite FAU.[12,17] In our parametric study, we tested different zinc sources and found that zinc acetate does not lead to FAU formation, whereas zinc nitrate and zinc oxide both produce ZnO-FAU. For this study, we report syntheses solely with ZnO owing to its significant enhancement of the crystallization rate (Figure S5). The choice of zinc source may also promote the formation of extra-framework particles instead of tetrahedrally incorporated zinc. This effect was observed previously[17] using $Zn(NO_3)_2$ and is similar to observations made in Sn-BEA syntheses using either $SnO_2$ or $SnCl_4$ as sources.[18] Comparison of multiple silicon sources revealed colloidal silica to be the most effective (Figures S6 and S7). The final optimized molar composition of the growth mixture selected for ZnO-FAU synthesis was 12 $SiO_2$: 1 $Al_2O_3$: 0.68 ZnO: 5 $Na_2O$: 160 $H_2O$.

The presence of zinc oxide alters the properties of FAU-type zeolite in several ways. There is a reduction in BET surface area (Table 1) for ZnO-FAU compared to in-house (FAU$_{syn}$) and commercial (FAU$_{com}$) zeolite Y prepared in the absence of zinc oxide (Figure S8). The surface area significantly increases after a mild acid wash (referred to herein as sample ZnO-FAU$_W$) due to the partial removal of extra-framework Al species (Figure 1B), any potential unreacted (amorphous) material, and a fraction of occluded ZnO. The presence of zinc oxide and a higher Si/Al ratio collectively improve zeolite stability owing to our observation that a similar acid wash of FAU prepared in house (sample FAU$_{syn,W}$) resulted in partial amorphization with concomitant loss of surface area and micropore volume (Table 1). These results indicate that ZnO-mediated synthesis of FAU-type zeolite improves its stability against acid treatment. Moreover, comparison of scanning electron microscope (SEM) images of ZnO-FAU (Figure 1C) and FAU$_{syn}$ (Figure 1D) reveal that the presence of zinc oxide leads to aggregates comprised of much smaller nanocrystals, which is consistent with slight peak broadening in powder XRD spectra (Figure S1).

Elemental analysis by X-ray photoelectron spectroscopy (XPS) that probes the outermost region (ca. 7 nm depth)[20] of particles reveals mild silicon zoning (i.e., higher Si/Al ratios on exterior surfaces)[21,22] for ZnO-FAU and ZnO-FAU$_W$ samples (Table S2). Comparison of Si/Al ratios for both samples

**Table 1. Physicochemical Properties of FAU-Type Zeolite Catalysts in This Study**

| | composition[a] | | | BET surface area[b] ($m^2$ $g^{-1}$) | | | acidity[c] ($\mu$mol $g^{-1}$) | |
|---|---|---|---|---|---|---|---|---|
| catalyst | Si/Al | Zn/Al | Zn/(Si + Al) | total | external | $V_{micro}$[b] ($cm^3$ $g^{-1}$) | Brønsted | Lewis |
| FAU$_{com}$[d] | 2.5 | NA[e] | NA | 761 | 45 | 0.29 | 711 | 489 |
| FAU$_{syn}$ | 2.5 | NA | NA | 749 | 45 | 0.29 | 723 | 328 |
| FAU$_{syn,W}$ | 2.6 | NA | NA | 372 | 72 | 0.13 | 311 | 223 |
| ZnO-FAU | 3.5 | 0.37 | 0.08 | 512 | 42 | 0.19 | 294 | 452 |
| ZnO-FAU$_W$ | 3.4 | 0.24 | 0.06 | 702 | 85 | 0.25 | 158 | 666 |

[a]Determined by EDS elemental analysis of faceted particles. [b]$N_2$ adsorption data with $V_{micro}$ obtained by the *t*-plot method. [c]Total acid site concentration calculated by $NH_3$ TPD multiplied by the percentage of each acid type from FTIR using pyridine adsorption with extinction coefficients of 1.67 cm/$\mu$mol and 2.22 cm/$\mu$mol for Brønsted and Lewis acid sites, respectively.[19] [d]Commercial zeolite Y from Zeolyst (CBV100). [e]NA = not applicable.


https://doi.org/10.1021/acsmaterialslett.2c00978
ACS Materials Lett. 2023, 5, 202−208

indicates that mild acid washing does not alter bulk composition (Table 1), but does slightly increase silicon content on exterior surfaces (Table S2). Additional analysis of the framework Si/Al ratio by solid-state $^{29}$Si MAS NMR (Figure S9) reveals a slight reduction from 3.7 to 3.4 after acid wash; however, transmission electron microscopy (TEM) images and electron diffraction patterns of samples before (Figure 2A) and after acid wash (Figure 2B) confirmed their

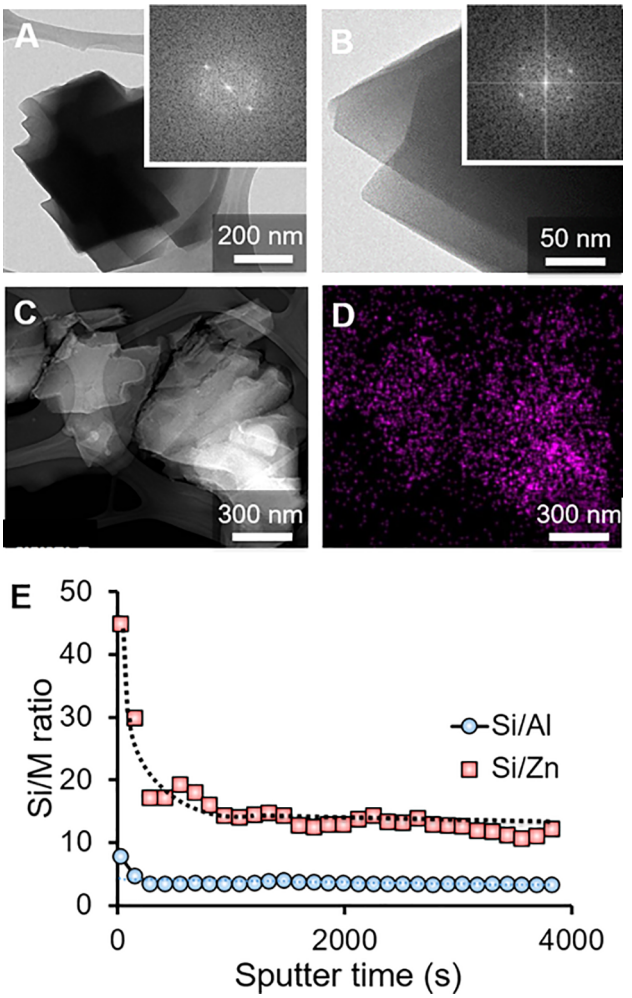


**Figure 2. (A and B) Representative transmission electron micrographs of (A) ZnO-FAU and (B) ZnO-FAU$_W$ samples. Insets show fast Fourier transforms of electron diffraction patterns. (C) High-angle angular dark field scanning transmission electron micrograph of ZnO-FAU$_W$. (D) Corresponding EDS elemental mapping of zinc. For additional TEM and EDS analyses of samples before and after acid washing, refer to Figures S11−S14. (E) ToF-SIMS analysis of Si/Zn and Si/Al ratios as a function of sputtering time for sample ZnO-FAU$_W$ (see Figure S15 for the same analysis of sample ZnO-FAU).**

crystallinity. High-angle angular dark field scanning transmission electron micrographs (Figure 2C) and corresponding elemental mapping (Figure 2D) reveal that Zn is uniformly distributed throughout the particle. This is consistent with time-of-flight secondary ion mass spectroscopy (ToF-SIMS) showing a monotonic reduction of Si/Zn ratio from the external surface to the interior (Figure 2E) with a relatively constant value of Si/Zn = 14 reached at longer sputtering times. XPS spectra of samples ZnO-FAU and ZnO-FAU$_W$ show a shift in the binding energy of Zn with respect to a reference ZnO material, indicating that zinc species are interacting with the zeolite framework (Figure S10).[23] The XPS peak in ZnO-FAU at 1022.2 eV is consistent with the presence of occluded ZnO nanoclusters,[24] which are likely responsible for the reduction in micropore volume (Table 1). For ZnO-FAU$_W$, a higher binding energy for Zn (1022.8 eV) and the observation of more isolated species in SEM-EDS (Figures S11−S14) indicates that washing with acid reduces the size of ZnO nanoclusters. The exact mechanism by which ZnO influences the Si/Al ratio of zeolite FAU is unknown. The observed increase in Si/Al ratio is likely due to a preferential coordination between silica and zinc. For instance, Anseau and co-workers[25] previously reported that anionic zinc species do not form complexes with aluminate, but compete with the latter for available silicate in zeolite growth media to generate zincosilicates. We posit that the presence of ZnO nanoclusters within FAU pores increases the local concentration of silicon, leading to a more siliceous product.

The nature of Zn speciation in FAU samples was characterized using multiple techniques. We first analyzed samples by UV−vis spectroscopy (Figure 3A) where the peak

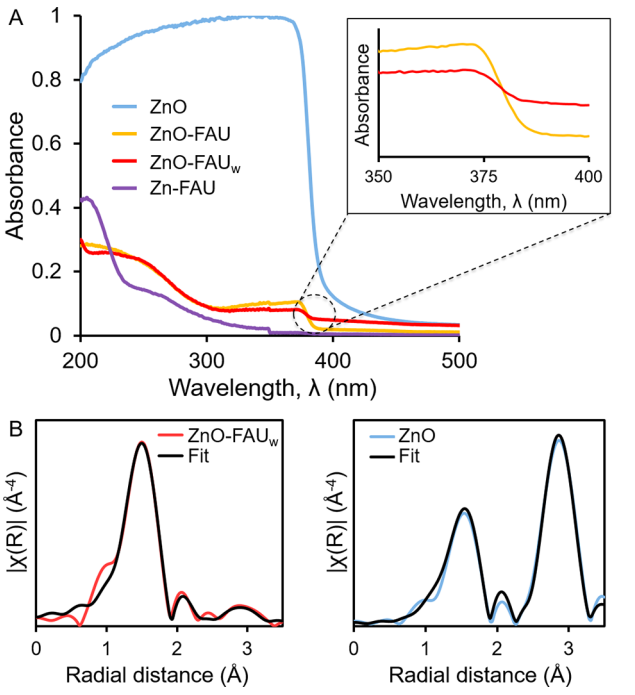


**Figure 3. (A) UV−vis spectra of the following samples: bulk ZnO reagent (reference) used as the source of ZnO in FAU syntheses, ZnO-FAU (before acid washing), ZnO-FAU$_W$ (after acid washing), and Zn-FAU. Callout: Enlarged region showing differences in bulk ZnO within zeolite samples before (yellow line) and after (red line) acid washing. (B) EXAFS spectra and model fits of samples ZnO-FAU$_W$ (left) and bulk ZnO (right). For the spectrum of sample Zn-FAU, refer to Figure S16.**

at 375 nm was identified as bulk ZnO by comparing zeolite samples to zinc oxide used as the reagent for syntheses. As expected, the amount of bulk ZnO in as-synthesized ZnO-FAU markedly decreases after acid washing (Figure 3A, inset), consistent with a decreased Zn/Al molar ratio and high solubility of ZnO at low pH (Table 1). The residual zinc within the zeolite does not occupy framework sites as


https://doi.org/10.1021/acsmaterialslett.2c00978
ACS Materials Lett. 2023, 5, 202−208

confirmed by UV−vis spectroscopy. More specifically, we compared ZnO-FAU$_W$ to another Zn-containing FAU (sample Zn-FAU) that was prepared by different synthesis conditions with a reduced zinc concentration (see the Methods for details). Framework $Zn^{2+}$ exhibits a peak around 200 nm[26] in UV−vis spectra (Figure 3A), which is observed for Zn-FAU but not for ZnO-FAU samples. Attempts to reduce zinc content via postsynthesis ion exchange were unsuccessful. Notably, elemental analysis showed that Si/Zn ratios are not altered by $NH_4^+$ ion exchange during the preparation of H-form zeolites for catalytic testing (*vide infra*). This suggests that extra-framework zinc cations are not present, but it remains possible that extra-framework (ZnO)−framework (Zn) pairings exist.[27]

To probe the local environment of Zn species, we used extended X-ray absorption fine structure spectroscopy (EXAFS) to assess the nearest and next nearest neighbors of $Zn^{2+}$, which were determined to be $O^{2-}$ and $Zn^{2+}$, respectively. Analysis of Zn K-edge (9659 eV) EXAFS spectra (Figure 3B) and coordination numbers of $Zn^{2+}$ with neighboring $O^{2-}$ and $Zn^{2+}$ (Table S3) reveal significant differences between ZnO-FAU$_W$ and bulk ZnO reference samples. For instance, Zn−Zn coordination numbers are 2.84 and 6.0, respectively. This suggests a different nature of zinc species in ZnO-FAU$_W$ that we posit are small clusters of ZnO owing to the lack of Zn−O−Si or Zn−O−Al coordination in models of EXAFS spectra that are observed in samples with framework Zn (e.g., Zn-FAU).[17] The exact structure of these ZnO clusters are unknown; however, there is precedent for such species to form in zeolites. For example, Chen et al.[28] report the formation of ZnO nanoclusters in both FAU and MFI pores as a result of postsynthesis wetness impregnation. In their study, they show these clusters possess properties that differ from bulk zinc oxide and interact noncovalently with the zeolite framework.

EXAFS data also reveal a reduction in the Zn−Zn coordination number from 4.0 before acid washing to 2.84 after washing, which is consistent with the loss of bulk ZnO. It is also interesting to note differences in acidity between samples prepared with and without zinc oxide (samples ZnO-FAU$_W$ and FAU$_{syn}$, respectively). The densities of Brønsted and Lewis acid sites were determined using a conventional method[29] of combined $NH_3$ temperature-programmed desorption (TPD) and pyridine FTIR titration (Table 1). The presence of zinc species enhances Lewis acidity; however, there is also a significant reduction in Brønsted acidity that cannot be explained by the increase in Si/Al ratio from 2.5 to 3.4. This seems to suggest that extra-framework zinc species alter Brønsted acid sites by either displacing $H^+$ or coordinating with the acid site, which is consistent with the reduction in strong acid sites (Table S4), although the exact reason for reduced Brønsted acidity is unknown.

Here we assess the impact that ZnO-mediated synthesis of zeolite FAU has on its hydrothermal stability and catalytic performance. To test hydrothermal stability, we performed mild steaming of H-form samples prepared without ZnO, using both in-house (FAU$_{syn}$) and commercial (FAU$_{com}$) faujasite, which were compared to sample ZnO-FAU$_W$. Zeolite powders were steamed at 400 °C for 1 h, whereupon the crystallinity was determined by powder XRD (Figure S17). As shown in Figure 4A, the resulting percent crystallinity of ZnO-FAU$_W$ (93%) is markedly higher than FAU$_{syn}$ (82%) for each of several tests, indicating that ZnO in synthesis media leads to

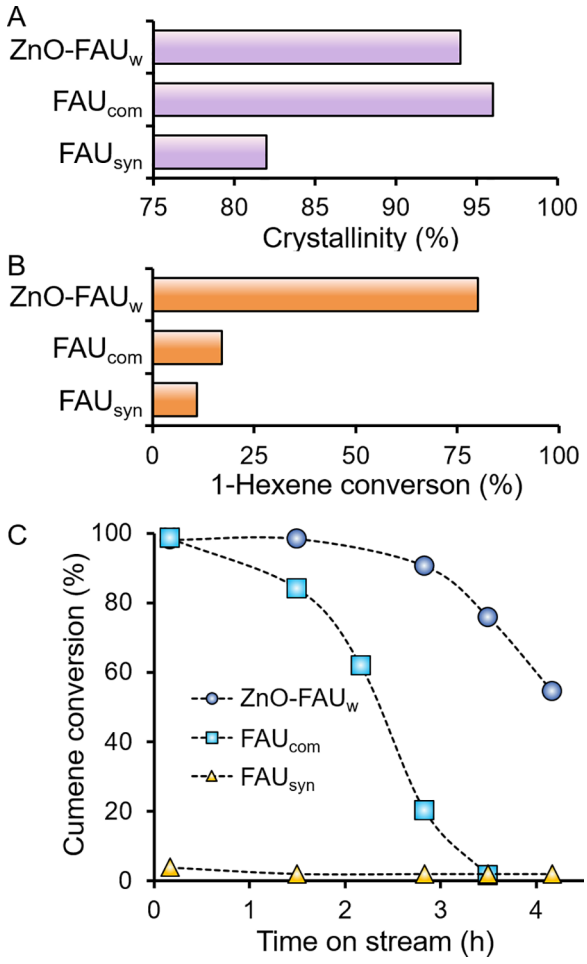


**Figure 4. (A) Percent crystallinity measured from powder XRD patterns after subjecting in-house (FAU$_{syn}$), commercial (FAU$_{com}$), and Zn-modified (ZnO-FAU$_W$) faujasite materials to mild steaming conditions (400 °C for 1 h). (B) Conversion of 1-hexene for each catalyst after a short contact time during 1-hexene cracking at 480 °C and catalyst-to-oil (CTO) ratio of 7.4. (C) Conversion of cumene as a function of time on stream for the cumene cracking reaction at 400 °C and weight-hourly space velocity, WHSV = 7.8 h$^{-1}$.**

materials with a hydrothermal stability comparable to that of the commercial sample (Zeolyst CBV100), which was used as a control owing to its similar Si/Al ratio as that of FAU$_{syn}$. The improved hydrothermal stability of ZnO-FAU$_W$ can be attributed, in large part, to its high Si/Al ratio. We also demonstrated that ZnO-FAU$_W$ is a superior catalyst for two different cracking reactions using a representative olefin (1-hexene) and aromatic (cumene). The conversion over ZnO-FAU$_W$ in 1-hexene cracking is more than 4-fold higher than both Zn-free catalysts (Figure 4B). For the cumene cracking reaction, we observe that in-house (FAU$_{syn}$) and commercial (FAU$_{com}$) catalysts exhibit stark differences in cumene conversion, which is not observed for 1-hexene cracking. The initial cumene conversion over ZnO-FAU$_W$ is equivalent to FAU$_{com}$; however, the time on stream behavior (Figure 4C) reveals that ZnO-FAU$_W$ has a much longer lifetime.

There are several reasons why ZnO-FAU$_W$ catalysts consistently demonstrate superior cracking performance. The first is with respect to its higher overall silicon content compared to commercial zeolite Y. For instance, it has been


https://doi.org/10.1021/acsmaterialslett.2c00978
ACS Materials Lett. 2023, 5, 202−208

demonstrated for multiple zeolites that a higher silicon content can prolong catalyst lifetime.[11,30] It is also possible that the presence of ZnO nanoclusters improves zeolite stability during calcination relative to Zn-free zeolites. We observed a higher fraction of extra-framework Al species in both reference samples ($FAU_{syn}$ and $FAU_{com}$) compared to ZnO-FAU (Figure S18), which may impact catalyst lifetime. An increase in Si/Al ratio from 2.5 to 3.4 would be expected to reduce the number of Brønsted acid sites by approximately 29%; however, the measured Brønsted acid site concentrations of samples $FAU_{com}$ (711 $\mu$mol $g^{-1}$) and ZnO-$FAU_W$ (158 $\mu$mol $g^{-1}$) indicate a 78% decrease in total sites (Table 1). This can be attributed to the presence of ZnO, which could either displace or interact with Brønsted acid sites without significantly altering surface area. Indeed, it has previously been reported that the formation of isolated $O^-[Zn(OH)]^+$ species can lead to a reduction in Brønsted acid site concentration.[24] The presence of ZnO increases the Lewis acidity wherein the role of these sites on catalyst activity is unknown but is difficult to directly assess due to the unique speciation of ZnO within the pores of ZnO-$FAU_W$ compared to bulk ZnO, $Zn^{2+}$ cation exchanged FAU, or framework zinc species. Although we cannot entirely rule out catalytic activity for ZnO nanoclusters, we did not observe an increase in aromatic products (Figure S19), which would be expected if ZnO species were active.[31] We additionally confirmed that using bulk ZnO as a catalyst leads to a negligible amount of 1-hexene conversion; therefore, it is unlikely that Zn species are responsible for the improved performance of ZnO-FAU. An unexpected outcome of ZnO-assisted FAU crystallization is the generation of a thin Si-zoned exterior rim (Si/Al = 9, Figure 2E). It has been shown that zeolites with siliceous surfaces exhibit longer lifetime via suppressed external reactions.[22,32] Recently, we have shown that core−shell zeolites MEL and MFI with Si-rich exterior shells have much longer lifetime in the methanol to hydrocarbons reaction owing, in part, to reduced external coking.[21] We posit that a similar effect contributes to the overall efficiency of ZnO-$FAU_W$ in cracking reactions. Si-zoning in faujasite is uncommon owing to the difficulty of preparing highly siliceous FAU zeolite; therefore, one practical advantage of using ZnO to generate Si-rich exterior surfaces is its single-step (i.e., one-pot) synthesis compared to alternative techniques (e.g., core−shells) that involve multistep syntheses.

In summary, we have demonstrated that the synthesis of faujasite in the presence of zinc oxide leads to a FAU-type zeolite with the highest reported silicon content from an organic-free medium. A combination of experimental techniques was used to confirm that ZnO is uniformly distributed within zeolite pores as extra-framework species that reduce Brønsted acidity and concomitantly increase Lewis acidity of ZnO-FAU. EXAFS data revealed that the ZnO species do not resemble bulk zinc oxide or framework zinc heteroatoms. We posit these extra-framework ZnO nanoclusters are occluded in zeolite micropores. These species, combined with the increased Si/Al ratio of the zeolite product, result in a significant enhancement of hydrothermal stability compared to samples prepared in the absence of ZnO. Moreover, catalytic cracking reactions confirm that ZnO-FAU exhibits a superior lifetime compared to in-house and commercial zeolite Y. Given the frequent challenges of creating Si-zoned materials and increasing Si/Al ratios of zeolites prepared in the absence of organic structure-directing agents, the findings in this study may lead to more generalizable synthesis methods for using ZnO (or other inorganic modifiers) to tailor the physicochemical properties of zeolites.

## ■ ASSOCIATED CONTENT

### Supporting Information

The Supporting Information is available free of charge at https://pubs.acs.org/doi/10.1021/acsmaterialslett.2c00978.

Materials and methods, supporting figures, and supporting tables (PDF)

## ■ AUTHOR INFORMATION


### Corresponding Author

**Jeffrey D. Rimer** − *Department of Chemical and Biomolecular Engineering, University of Houston, Houston, Texas 77204, United States;* orcid.org/0000-0002-2296-3428; Email: jrimer@central.uh.edu

### Authors

**Deependra Parmar** − *Department of Chemical and Biomolecular Engineering, University of Houston, Houston, Texas 77204, United States*

**Adam J. Mallette** − *Department of Chemical and Biomolecular Engineering, University of Houston, Houston, Texas 77204, United States*

**Noemi Linares** − *Molecular Nanotechnology Lab, Department of Inorganic Chemistry, University of Alicante, 03690 San Vicente del Raspeig, Alicante, Spain;* orcid.org/0000-0001-9376-2984

**Sarah A. Saslow** − *Earth Systems Science Division, Energy and Environment Directorate, Pacific Northwest National Laboratory, Richland, Washington 99352, United States;* orcid.org/0000-0002-8385-2676

**Tanguy Terlier** − *Shared Equipment Authority, SIMS Laboratory, Rice University, Houston, Texas 77005, United States*

**James J. Strohm** − *Albemarle Corporation, Pasadena, Texas 77507, United States*

**Lee P. Barber** − *Albemarle Corporation, Pasadena, Texas 77507, United States*

**Heng Dai** − *Albemarle Corporation, Pasadena, Texas 77507, United States*

**Javier García-Martínez** − *Molecular Nanotechnology Lab, Department of Inorganic Chemistry, University of Alicante, 03690 San Vicente del Raspeig, Alicante, Spain;* orcid.org/0000-0002-7089-4973

Complete contact information is available at: https://pubs.acs.org/10.1021/acsmaterialslett.2c00978


### Author Contributions

CRediT: **Deependra Parmar** conceptualization, data curation, formal analysis, investigation, methodology, writing-original draft, writing-review & editing; **Adam J. Mallette** data curation, formal analysis, investigation, writing-original draft, writing-review & editing; **Noemi Linares** data curation, formal analysis, visualization, writing-review & editing; **Sarah A. Saslow** data curation, formal analysis, methodology; **Tanguy Terlier** data curation, resources; **James J. Strohm** formal analysis, resources; **Lee P. Barber** data curation, resources; **Heng Dai** data curation, formal analysis, resources; **Javier García-Martínez** methodology, project administration, resources, writing-review & editing; **Jeffrey D Rimer** conceptualiza-



https://doi.org/10.1021/acsmaterialslett.2c00978
ACS Materials Lett. 2023, 5, 202−208

tion, funding acquisition, project administration, supervision, writing-original draft, writing-review & editing.

### Notes

The authors declare no competing financial interest.

## ■ ACKNOWLEDGMENTS

J.D.R. received funding primary from the National Science Foundation (Award DMR-2005201) and additional support from The Welch Foundation (Award E-1794). We also wish to thank Albemarle Corporation for their support of this work. J.G.M. and N.L. received funding from the European Union's Horizon 2020 research and innovation program under grant agreement No. 872102 and the Spanish MINECO and AEI/FEDER, UE, through Project ref. RTI2018-099504-B-C21. N.L. also acknowledges the University of Alicante support (UATALENTO17-05). ToF-SIMS analysis was carried out with support provided by the National Science Foundation (Award CBET-1626418). This work was conducted in part using resources of the Shared Equipment Authority at Rice University. This research used resources of the Advanced Photon Source, a U.S. Department of Energy (DOE) Office of Science user facility operated for the DOE Office of Science by Argonne National Laboratory under Contract No. DE-AC02-06CH11357. The authors thank Mahalingam Balasubramanian from APS Sector 20 (now at Oak Ridge National Laboratory) for collecting the EXAFS dataset.

## ■ REFERENCES

(1) Csicsery, S. M. Shape-selective catalysis in zeolites. *Zeolites* **1984**, *4* (3), 202−213. Caro, J.; Noack, M.; Kolsch, P.; Schafer, R. *Microporous Mesoporous Mater.* **2000**, *38*, 3−24. Vermeiren, W.; Gilson, J.-P. Impact of zeolites on the petroleum and petrochemical industry. *Top. Catal.* **2009**, *52* (9), 1131−1161.

(2) Shi, J.; Wang, Y.; Yang, W.; Tang, Y.; Xie, Z. Recent advances of pore system construction in zeolite-catalyzed chemical industry processes. *Chem. Soc. Rev.* **2015**, *44* (24), 8877−8903. Vogt, E. T.; Weckhuysen, B. M. Fluid catalytic cracking: recent developments on the grand old lady of zeolite catalysis. *Chem. Soc. Rev.* **2015**, *44* (20), 7342−7370.

(3) Frising, T.; Leflaive, P. Extraframework cation distributions in X and Y faujasite zeolites: A review. *Microporous Mesoporous Mater.* **2008**, *114* (1−3), 27−63.

(4) Magee, J. S.; Mitchell, M. M. *Fluid Catalytic Cracking: Science and Technology*; Elsevier, 1993. Maher, P. K.; McDaniel, C. V. Preparation of thermal stable synthetic zeolites. US Patent US3518051A, 1970. Chawla, A.; Linares, N.; Rimer, J. D.; García-Martínez, J. Time-resolved dynamics of intracrystalline mesoporosity generation in USY zeolite. *Chem. Mater.* **2019**, *31* (14), 5005−5013. Li, K.; Valla, J.; Garcia-Martinez, J. Realizing the commercial potential of hierarchical zeolites: new opportunities in catalytic cracking. *ChemCatChem.* **2014**, *6* (1), 46−66.

(5) Beyer, H. K.; Belenykaja, I. M.; Hange, F.; Tielen, M.; Grobet, P. J.; Jacobs, P. A. Faraday Transactions 1: Physical Chemistry in Condensed Phases. Preparation of high-silica faujasites by treatment with silicon tetrachloride. *J. Chem. Soc., Faraday Trans.* **1985**, *81* (11), 2889−2901. Fleisch, T.; Meyers, B.; Ray, G.; Hall, J.; Marshall, C. Hydrothermal dealumination of faujasites. *J. Catal.* **1986**, *99* (1), 117−125. Lutz, W. Zeolite Y: synthesis, modification, and properties—a case revisited. *Adv. Mater. Sci. Eng.* **2014**, 724248.

(6) Zhu, D.; Wang, L.; Zhang, W.; Fan, D.; Li, J.; Cui, W.; Huang, S.; Xu, S.; Tian, P.; Liu, Z. Realizing Fast Synthesis of High-Silica Zeolite Y with Remarkable Catalytic Performance. *Angew. Chem. Int. Chem.* **2022**, *61*, e202117698.

(7) Delprato, F.; Delmotte, L.; Guth, J.; Huve, L. Synthesis of new silica-rich cubic and hexagonal faujasites using crown-etherbased supramolecules as templates. *Zeolites* **1990**, *10* (6), 546−552. Dougnier, F.; Patarin, J.; Guth, J.; Anglerot, D. Synthesis, characterization, and catalytic properties of silica-rich faujasite-type zeolite (FAU) and its hexagonal analog (EMT) prepared by using crown-ethers as templates. *Zeolites* **1992**, *12* (2), 160−166.

(8) Ke, Q.; Khalil, I.; Smeyers, B.; Li, Z.; de Oliveira-Silva, R.; Sels, B.; Sakellariou, D.; Dusselier, M. A Cooperative OSDA Blueprint for Highly Siliceous Faujasite Zeolite Catalysts with Enhanced Acidity Accessibility. *Angew. Chem.* **2021**, *133* (45), 24391−24399.

(9) Zhu, D.; Wang, L.; Fan, D.; Yan, N.; Huang, S.; Xu, S.; Guo, P.; Yang, M.; Zhang, J.; Tian, P.; Liu, Z. A Bottom-Up Strategy for the Synthesis of Highly Siliceous Faujasite-Type Zeolite. *Adv. Mater.* **2020**, *32* (26), 2000272.

(10) Reiprich, B.; Tarach, K. A.; Pyra, K.; Grzybek, G.; Góra-Marek, K. High-Silica Layer-like Zeolites Y from Seeding-Free Synthesis and Their Catalytic Performance in Low-Density Polyethylene Cracking. *ACS Appl. Mater. Interfaces* **2022**, *14* (5), 6667−6679. Ferdov, S.; Marques, J.; Tavares, C. J.; Lin, Z.; Mori, S.; Tsunoji, N. UV-light assisted synthesis of high silica faujasite-type zeolite. *Microporous Mesoporous Mater.* **2022**, *336*, 111858.

(11) Oleksiak, M. D.; Muraoka, K.; Hsieh, M. F.; Conato, M. T.; Shimojima, A.; Okubo, T.; Chaikittisilp, W.; Rimer, J. D. Organic-Free Synthesis of a Highly Siliceous Faujasite Zeolite with Spatially Biased $Q^4$ (nAl) Si Speciation. *Angew. Chem.* **2017**, *129* (43), 13551−13556.

(12) Guo, Y.; Sun, T.; Gu, Y.; Liu, X.; Ke, Q.; Wang, S. Organic-Free, ZnO-Assisted Synthesis of Zeolite FAU with Tunable $SiO_2$/$Al_2O_3$ Molar Ratio. *Chem. Asian J.* **2018**, *13* (9), 1114−1118.

(13) Meng, B.; Ren, S.; Li, Z.; Nie, S.; Zhang, X.; Song, W.; Guo, Q.; Shen, B. A facile organic-free synthesis of high silica zeolite Y with small crystal in the presence of $Co^{2+}$. *Microporous Mesoporous Mater.* **2021**, *323*, 111248.

(14) Li, J.; Corma, A.; Yu, J. Synthesis of new zeolite structures. *Chem. Soc. Rev.* **2015**, *44* (20), 7112−7127. Wu, Q.; Xu, C.; Zhu, L.; Meng, X.; Xiao, F.-S. Recent strategies for synthesis of metallosilicate zeolites. *Catal. Today* **2022**, *390-391*, 2−11. Kolyagin, Y. G.; Yakimov, A. V.; Tolborg, S.; Vennestrøm, P. N.; Ivanova, I. I. Tuning of Sn-BEA Reactivity by Controlling Tin Location in the BEA Framework. *J. Phys. Chem. C* **2021**, *125* (48), 26679−26687.

(15) Maldonado, M.; Oleksiak, M. D.; Chinta, S.; Rimer, J. D. Controlling crystal polymorphism in organic-free synthesis of Na-zeolites. *J. Am. Chem. Soc.* **2013**, *135* (7), 2641−2652.

(16) Gu, X.; Dong, J.; Nenoff, T. M. Synthesis of defect-free FAU-type zeolite membranes and separation for dry and moist $CO_2/N_2$ mixtures. *Ind. Eng. Chem. Res.* **2005**, *44* (4), 937−944. Zhang, F.; Xu, L.; Hu, N.; Bu, N.; Zhou, R.; Chen, X. Preparation of NaY zeolite membranes in fluoride media and their application in dehydration of bio-alcohols. *Sep. Purif. Technol.* **2014**, *129*, 9−17.

(17) Mallette, A. J.; Hong, S.; Freeman, E. E.; Saslow, S. A.; Mergelsberg, S.; Motkuri, R. K.; Neeway, J. J.; Mpourmpakis, G.; Rimer, J. D. Heteroatom Manipulation of Zeolite Crystallization: Stabilizing Zn-FAU against Interzeolite Transformation. *JACS Au* **2022**, *2*, 2295−2306.

(18) Tolborg, S.; Katerinopoulou, A.; Falcone, D. D.; Sádaba, I.; Osmundsen, C. M.; Davis, R. J.; Taarning, E.; Fristrup, P.; Holm, M. S. Incorporation of tin affects crystallization, morphology, and crystal composition of Sn-Beta. *Journal of Materials Chemistry A* **2014**, *2* (47), 20252−20262.

(19) Emeis, C. A. Determination of Integrated Molar Extinction Coefficients for Infrared Absorption Bands of Pyridine Adsorbed on Solid Acid Catalysts. *J. Catal.* **1993**, *141* (2), 347−354.

(20) Stöcker, M. X-ray photoelectron spectroscopy on zeolites and related materials. *Micropor. Mater.* **1996**, *6* (5−6), 235−257.

(21) Le, T. T.; Chawla, A.; Rimer, J. D. Impact of acid site speciation and spatial gradients on zeolite catalysis. *J. Catal.* **2020**, *391*, 56−68.

(22) Wang, C.; Zhang, L.; Huang, X.; Zhu, Y.; Li, G. K.; Gu, Q.; Chen, J.; Ma, L.; Li, X.; He, Q.; et al. Maximizing sinusoidal channels of HZSM-5 for high shape-selectivity to p-xylene. *Nat. Commun.* **2019**, *10* (1), 4348.



https://doi.org/10.1021/acsmaterialslett.2c00978
ACS Materials Lett. 2023, 5, 202−208

(23) Niu, X.; Gao, J.; Miao, Q.; Dong, M.; Wang, G.; Fan, W.; Qin, Z.; Wang, J. Influence of preparation method on the performance of Zn-containing HZSM-5 catalysts in methanol-to-aromatics. *Microporous Mesoporous Mater.* **2014**, *197*, 252−261.
(24) Gabrienko, A. A.; Arzumanov, S. S.; Toktarev, A. V.; Danilova, I. G.; Prosvirin, I. P.; Kriventsov, V. V.; Zaikovskii, V. I.; Freude, D.; Stepanov, A. G. Different Efficiency of $Zn^{2+}$ and ZnO Species for Methane Activation on Zn-Modified Zeolite. *ACS Catal.* **2017**, *7* (3), 1818−1830.
(25) Anseau, M. R.; Leung, J. P.; Sahai, N.; Swaddle, T. W. Interactions of silicate ions with zinc (II) and aluminum (III) in alkaline aqueous solution. *Inorg. Chem.* **2005**, *44* (22), 8023−8032.
(26) Wang, L.; Sang, S.; Meng, S.; Zhang, Y.; Qi, Y.; Liu, Z. Direct synthesis of Zn-ZSM-5 with novel morphology. *Mater. Lett.* **2007**, *61* (8−9), 1675−1678.
(27) Koike, N.; Iyoki, K.; Wang, B.; Yanaba, Y.; Elangovan, S. P.; Itabashi, K.; Chaikittisilp, W.; Okubo, T. Increasing the ion-exchange capacity of MFI zeolites by introducing Zn to aluminosilicate frameworks. *Dalton Transactions* **2018**, *47* (28), 9546−9553. Iyoki, K.; Itabashi, K.; Okubo, T. Seed-Assisted, One-Pot Synthesis of Hollow Zeolite Beta without Using Organic Structure-Directing Agents. *Chem-Asian J.* **2013**, *8* (7), 1419−1427.
(28) Chen, J.; Feng, Z.; Ying, P.; Li, C. ZnO clusters encapsulated inside micropores of zeolites studied by UV Raman and laser-induced luminescence spectroscopies. *J. Phys. Chem. B* **2004**, *108* (34), 12669−12676.
(29) Jain, R.; Chawla, A.; Linares, N.; García Martínez, J.; Rimer, J. D. Spontaneous pillaring of pentasil zeolites. *Adv. Mater.* **2021**, *33* (22), 2100897.
(30) Gao, Y.; Zheng, B.; Wu, G.; Ma, F.; Liu, C. Effect of the Si/Al ratio on the performance of hierarchical ZSM-5 zeolites for methanol aromatization. *RSC Adv.* **2016**, *6* (87), 83581−83588. Kianfar, E.; Hajimirzaee, S.; Mousavian, S.; Mehr, A. S. Zeolite-based catalysts for methanol to gasoline process: a review. *Microchem. J.* **2020**, *156*, 104822.
(31) Zhang, C.; Kwak, G.; Lee, Y.-J.; Jun, K.-W.; Gao, R.; Park, H.-G.; Kim, S.; Min, J.-E.; Kang, S. C.; Guan, G. Light hydrocarbons to BTEX aromatics over Zn-modified hierarchical ZSM-5 combined with enhanced catalytic activity and stability. *Microporous Mesoporous Mater.* **2019**, *284*, 316−326.
(32) Henry, M.; Bulut, M.; Vermandel, W.; Sels, B.; Jacobs, P.; Minoux, D.; Nesterenko, N.; Dath, J. Low temperature conversion of linear $C_4$ olefins using acid ZSM-5 zeolites with aluminum concentration gradient. *Appl. Catal. A: Gen.* **2012**, *437*, 96−103. Mores, D.; Stavitski, E.; Verkleij, S. P.; Lombard, A.; Cabiac, A.; Rouleau, L.; Patarin, J.; Simon-Masseron, A.; Weckhuysen, B. M. Core−shell H-ZSM-5/silicalite-1 composites: Brønsted acidity and catalyst deactivation at the individual particle level. *Phys. Chem. Chem. Phys.* **2011**, *13* (35), 15985−15994.




https://doi.org/10.1021/acsmaterialslett.2c00978
*ACS Materials Lett.* 2023, 5, 202−208